JOURNAL OF MATERIALS SCIENCE **34** (1999) 897–904

Stress transfer in dilute short-fibre reinforced composites

V. I. RÄISÄNEN, H. J. HERRMANN
ICA1, Universität Stuttgart, Pfaffenwaldring 27, D-70569 Stuttgart, Germany
E-mail: ura@fyslab.hut.fi

Numerical calculations for stress transfer between a single fibre and a surrounding three-dimensional elastic medium are presented. We study systematically the effect of fibre parameters on stress transfer between the fibre and the matrix. We pay special attention to fibres at an oblique angle with respect to the external strain, as well as to the case of a fibre breaking into two parts of equal size at the middle. According to the simulations, for a small ratio of elastic moduli of the fibre and the matrix, $\delta = E_f/E_{bg}$, the largest stresses are seen near the breaking point of the fibre for the latter case. For short fibres, δ has little effect on pressure increase next to the breaking point. This is due to the fibres being shorter than the critical length. For such short fibres, the numerical results for the maximal axial stress are in agreement with a logarithmic dependence on δ. © *1999 Kluwer Academic Publishers*

1. Introduction

The elastic properties of long-fibre reinforced composites are well understood theoretically [1]. More recently, the effect of fibre fracture in long-fibre composites has been studied with numerical simulations using Green's lattice functions method [2–4]. From a technological viewpoint, however, the use of long fibres is not a cost-effective way of reinforcing materials. Subsequently, the micromechanics of composites consisting of either a random or textured placement of short fibres embedded in a matrix is an active field of research. Often the mechanical properties of composites are calculated by studying stress transfer between a fibre and the matrix. From the physics point of view, this *stress transfer analysis* reflects the fact that at different locations in the fibre–matrix interface, a varying amount of stress is transferred to the fibre from the matrix. As an example of stress transfer thinking, Cox's [5] so-called shear-lag model appears to be a good way of predicting the mechanical properties of composites for low strains and small volume fractions of fibres [6].

The shear-lag theory yields the following prediction for axial stress in the fibre as a function of the axial co-ordinate, $\sigma_f(x)$

$$\sigma_f(x) = E_f \epsilon_x \left(1 - \frac{\cosh gx/w_f}{\cosh \beta l_f/w_f}\right) \quad (1)$$

Above, l_f and w_f are the length and the width of the fibre, the axial coordinate $x \in [-l_f/2, l_f/2]$ and the constant g is given by

$$g = \left(\frac{2G_m}{E_f \gamma}\right)^{1/2} \quad (2)$$

Above, G_m is the shear modulus of the matrix, E_f is the elastic modulus of the fibres and γ is a geometrical factor dependent on the placement of fibres and volume fraction (i.e. the number of fibres) thereof.

When strains are large enough to give rise to rupture in the fibre–matrix interface, the predictive power of the shear-lag model is weakened considerably. Interactions between the stress fields of individual fibres render the effective medium approximation-type theories insufficient for use in predicting the mechanical properties of composites where the volume fraction of fibres is high. In addition, axial stress transfer–not accounted for by the original shear-lag theory–has been shown to take place near fibre ends [7, 8]. Recently, extensions to the shear-lag theory have been proposed, which also take into account axial stress transfer [9, 10].

The mechanics of a system consisting of a matrix and of single fibres aligned in the direction of external strain have previously been studied numerically using discrete representation of the elastic problem [7, 11–16]. In addition, finite element modelling of the immediate surroundings of a fibre has been used, e.g. to address interfacial stresses [17, 18]. Simulations have been employed to study subjects like elastic modulus of the composite [11, 12] and stress transfer between the matrix and the fibres [7, 11–13]. A major motivation in the study of systems consisting of a single fibre in a matrix has been the applicability of shear-lag-type models and the study of the dependence of the critical length on the ratio of the elastic moduli of the fibre and the matrix. (The critical length is essentially the length of that part of the fibre that does not carry full load [6].) Previously cited results have been presented for fibres that are longer than the critical length.

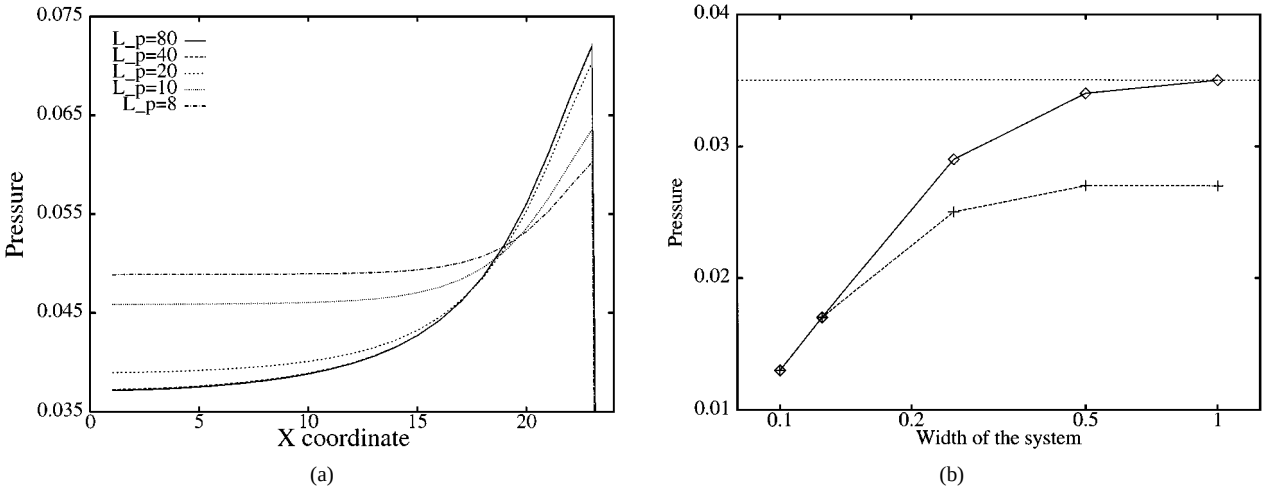

Figure 1 (a) Dependence of stresses in the matrix in a cut taken along the length of the fibre. (b) The perpendicular stresses at the edge of the system ($\diamond$) and next to the fibre (+). In both cases, the ratio of the elastic modulus of the fibre and the matrix $E_{\rm f}/E_{\rm bg} = 8$ and the length of the system in the x-direction is $L_x = 80$. In (b), the width of the system is given in units of L_x. Please note that in this figure, the external strain, $\epsilon_x = 0.035$, has been applied instead of the smaller value used later.

In this work we present results for changes in the stress field of a matrix around a single fibre with perfect bonding between the fibre and the matrix. The stress state of the matrix is modelled using pressure, p. Technically, pressure is defined as the first invariant of the stress tensor, T, or

$$p' = \frac{1}{3}\mathrm{Tr}T = \frac{1}{3}(\sigma_1 + \sigma_2 + \sigma_3) \qquad (3)$$

in the principal stress co-ordinates. In the following, we use the variable $p = 3p'$ (i.e. total pressure) as a convenient scalar measure to characterize the stress state of the matrix.

In Section 2, the numerical models used are presented. The results of the simulations for fibres in the direction of external strain are shown in Section 3.1. and those for fibres at an oblique angle in Section 3.2. A subject of interest with respect to experiments, we study the effect of fibre breaking in Section 3.3. Our conclusions are drawn together in Section 4.

2. Numerical model

For numerical simulations we have used a linearized bond bending network in three dimensions. The network consists of a simple cubic arrangement of bonds in a regular lattice. The bonds have bending stiffness in addition to spring stiffness. The discretation scheme can be viewed as a coarse-grained representation of the micromechanics of a solid material on large length scales [19]. We chose to use bond bending because the spring model (vanishing bending stiffness) suffers from the drawback that its Poisson's constant is zero [7–20], and the shear modulus vanishes for a non-perturbed hypercubic lattice [19]. Another alternative, the beam model, is a discretation of Cosserat-type elasticity [21, 22]. However, we need not consider local rotational degrees of freedom in our studies, whereby we use a simpler model. We have chosen the bending stiffness of the bonds in such a way that the *microscopic* Poisson's constant for the matrix is $\nu = 0.3$.

We have studied the effect of system width on stress transfer to determine appropriate system dimensions for the simulations (Fig. 1). In the figure, the curve $L_{\rm p} = 20$ corresponds to the system width used by Termonia [13]. The results differ (albeit only slightly) from the "infinite system width" limit ones at $\delta = E_{\rm f}/E_{\rm bg} = 8$; the largest stiffness of the fibre used in Termonia's work was $\delta = 20$. Direct comparison between different types of models is beyond the scope of this article, but we note the previous fact to illustrate the situation specific to our model. In finite element models for shear stress transfer, the simulated system often consists of a cylindrical region of matrix around the fibre. In these models, the radius of the cylinder is sometimes only twice that of the matrix, although $\delta \approx 6$ [17, 18]. To attain results independent of lattice size, we chose to use a lattice of size L^3 with $L = 80$ (the maximum fibre length used was $l_{\rm f} = 32 \times a$, where a is the lattice spacing).

The lattice is strained by uniaxial elongation in the [1 0 0] direction, and has periodic boundary conditions in the [0 1 0] and [0 0 1] directions. The fibre was modelled as having width, $w_{\rm f}$, and length, $l_{\rm f}$ (both multiples a), and being located at the centre of the simulation volume oriented either in the [1 0 0] direction or at an angle of $\pi/4$ in the plane spanned by the [1 0 0] and [0 1 0] directions (see Fig. 2). The values $l_{\rm f} = 4 - 32 \times a$, and $w_{\rm f} = a$ and $2a$ were used for fibres parallel to external strain. For tilted fibres, the projection of the fibre length in the direction of the external strain, $l_{\rm f}^x$, and the projection of fibre width, $w_{\rm f}^x$, were varied within the same limits. The width of the fibre is an effective one, i.e. for a one-dimensional sequence of bonds $w_{\rm f} = a$. The elastic modulus of the fibre (with respect to that of the matrix) is determined by the elastic constants of the beams constituting the fibre (matrix). The elastic modulus of the matrix is $E_{\rm bg} = 1$, whereas for the fibres the corresponding quantity is $E_{\rm f}$.

An external strain of the magnitude $\epsilon_x = 0.01$ was imposed on the system. The actual magnitude of the strain is irrelevant as we use small strain theory, i.e. linear elasticity. The mechanical equilibrium of the system was solved with a simple sequential over-relaxation technique. This method is deemed sufficient because

the system does not contain disorder whereby convergence is quick and there is no need to do an ensemble average over disorder. The scan of the entire parameter range for $L = 80$ on a Sun SPARCstation took a few hours of computer processing time.

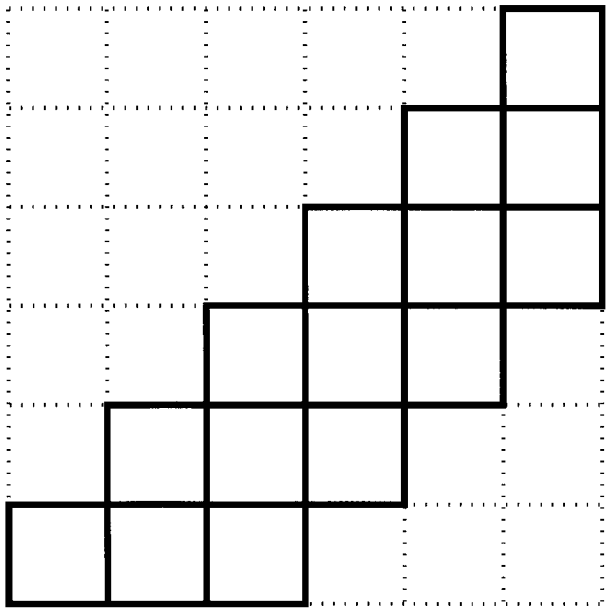

Figure 2 A schematic of the two-dimensional discrete representation of a tilted fibre at an angle of $\pi/4$. The projected width, $w_f^x = 4a$.

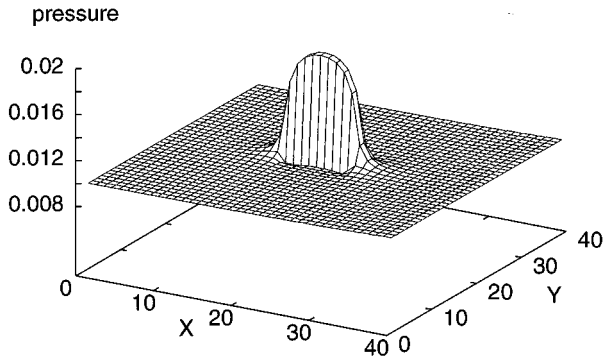

Figure 3 Pressure field in a $x-y$-directional slice through the system at $z = L/2$ with $L = 40$, $l_f = 8a$ and $w_f = 2a$. The elastic modulus of the fibre $E_f = 2E_{bg}$.

Fig. 3 shows an example of the stresses in the system. The physical quantity depicted is p.

In the figure, both the distribution of axial stresses along a fibre as well as the pressure in the neighbouring matrix points are clearly visible. The axial stress in the fibre, σ_f, exhibits a typical form in which the stress decays at the ends of the fibre and has a maximum at the middle. The fibre shown in Fig. 3 is short, $l_f = 8a$, whereby it does not carry as much load as it could. In traditional composite research parlance, the critical fibre length $l_c > l_f$.

3. Discussion

3.1. Longitudinal fibres

In the first part of this section, we discuss the matrix pressure and the shape of the stress field around a fibre. In the following, we denote the magnitude of pressure increase at fibre ends by α and decrease at the middle of the fibre by β. Data for the dependence of these quantities of the ratio of the elastic moduli of the fibres and the matrix δ, as well as fibre length and width l_f and w_f, are presented.

3.1.1. Matrix pressure

To obtain quantitative measures for pressure changes in the matrix, we have studied one-dimensional cuts of the pressure in the system near the fibre. The first such cut is taken along the fibre axis, i.e. in the [1 0 0] direction, and the second one perpendicular to the fibre in the [0 1 0] direction at the middle of the system. Stresses at the ends of the fibre increase as the ratio E_f/E_{bg} grows, indicative of axial stress transfer becoming more and more important with stiffer fibres. Similarly, an increase in fibre width yields higher stresses in the matrix.

In Fig. 4 the pressure at the fibre–matrix interface is plotted. The quantity is made mesh independent by measuring the pressure exactly at the node, which is shared both by the fibre and the matrix. In general, the pressure at fibre ends grows with l_f until l_c. After that, the growth of the value slows down, being an indication of possible pressure saturation. For $\delta > 1$, the increase in pressure becomes a non-linear function of δ. The

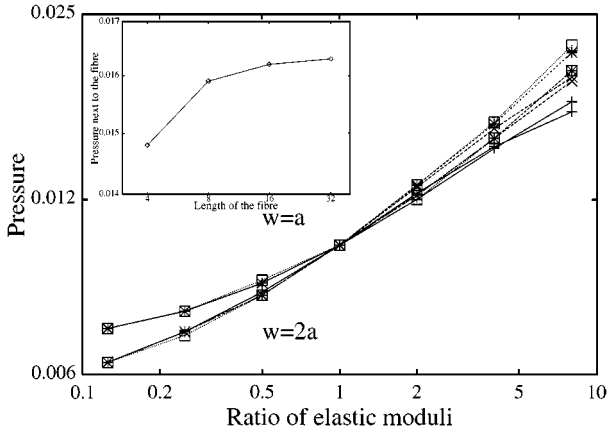

(a)

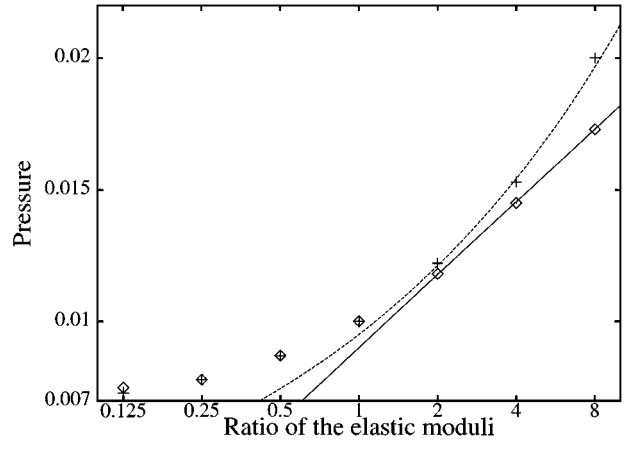

(b)

Figure 4 (a) Log–log plot of matrix pressure at the ends of the fibre ($\alpha \times p_{bg}$) as a function of δ: (——) $l_f = 4a$; (---) $l_f = 8a$; (· · ·) $l_f = 16a$; (-·-·-·-) $l_f = 32a$. Inset: the same quantity as a function of l_f for $\delta = 4$ and $w_f = 2a$. (b) The same quantity, but only the cases $l_f = 4a$ (◇) and $l_f = 32a$ (+) plotted on a log-linear scale. $w_f = 2a$ in both cases. The upper line represents a best fit to points $\delta = 2 - 8a$.

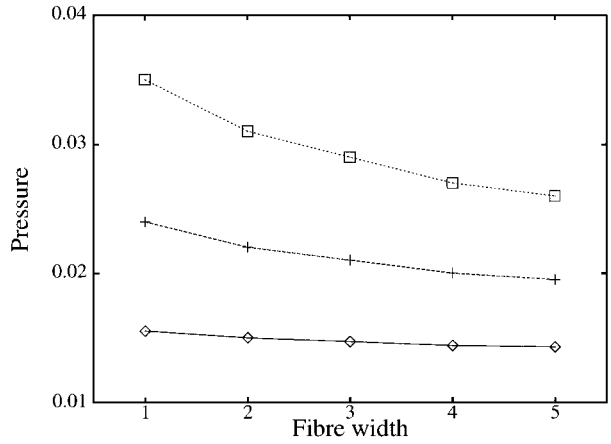

Figure 5 Effect of fibre width on pressure increase. $l_f = 32$; curves correspond to (bottom to top) $\delta = 2$, 4 and 8.

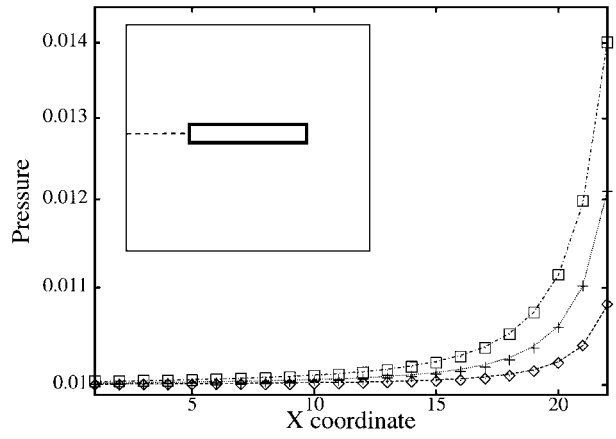

Figure 6 Pressure in the matrix in the vicinity of the fibre end. Shown is pressure along a line oriented in the direction of the fibre axis and located at the middle of the lattice (see inset). Points represent numerical results and lines the predictions given by Equation 4. (□) $\delta = 8$; (+) $\delta = 4$; (◇) $\delta = 2$. In all cases, $L = 80$, $l_f = 32a$ and $w_f = 2a$.

relation between the pressure increase and the ratio of elastic moduli is approximately $\alpha \propto \delta^{0.35}$. This scaling is roughly in accord with the results of Termonia [13]. For fibre lengths shorter than the critical value, the dependence is approximately logarithmic.

The pressure increase in the matrix is slightly smaller than that shown by finite difference modelling [13], and is clearly lower than that obtained by the imaginary fibre method [10]. The former fact may be caused either by the small system width used by Termonia or be purely a consequence of the difference between numerical models used.

The effect of increasing fibre width on pressure *per unit volume* next to the fibre end is negative (Fig. 5). The general tendency is the same for all fibre lengths.

For perpendicular stress changes the effect of fibre length is opposite to that seen at fibre ends: the longer the fibre, the smaller the change. This follows simply from the change in the pressure field of the fibre being distributed over a larger area in the matrix when the fibre is longer. The effects of fibre width, elastic modulus and length are similar to those in Fig. 4. The largest pressure reductions in our simulations are roughly 25%, whereas the largest increases at fibre ends are in excess of 100% for $l_f = 32 \times a$ and $E_f = 8 \times E_{bg}$.

3.1.2. Far field of the fibre

In what follows, we study the far field due to the fibre. On the basis of the results presented, one expects the model to reflect both pressure increase next to the fibre ends and pressure decrease towards the middle of the fibre. Furthermore, the results are compatible with dipole-like decay of the pressure field. From these preliminary observations, a simple Ansatz of the form

$$p(\boldsymbol{x}) = \mathrm{c}(l_f, w_f, \delta) \int 3\frac{|\boldsymbol{p}_0 \times \boldsymbol{r}|^2 - 1}{|\boldsymbol{x} - \boldsymbol{x}'|^4} - \frac{\mathrm{d}(l_f, w_f)}{|\boldsymbol{x} - \boldsymbol{x}'|^3}\,\mathrm{d}x' \tag{4}$$

may be constructed, which indeed produces promising results (Fig. 6). Above, the constants $\mathrm{c}(l_f, w_f, \delta)$ and $\mathrm{d}(l_f, w_f)$ include the explicit dependence on these quantities; $\boldsymbol{p}_0$ is a unit vector in the direction of the external strain and d is a constant. Also for perpendicular stresses (not shown here) the dipole form is accurate within a few per cent. Please note that the scheme described above only gives the approximate shape of the stress field and l_f, w_f and δ-dependence must be taken care of "by hand". In summary, the dipole approximation for the fibre shape effect applies for fibres of zero as well as finite width.

3.1.3. Stress transfer at the fibre–matrix interface

In Fig. 7 we show the interfacial shear stresses between the fibre and the matrix next to the fibre ends. The quantity depicted is σ_{xy}, the shear stress in bonds perpendicular to the fibre as obtained from the numerical model. As can be expected, the interfacial stresses are in accord with the results for axial stress transfer at fibre ends, i.e. they are not affected by the fibre length when $l_f > l_c$. The magnitude of σ_{xy} may be compared with the trace of σ depicted in Fig. 4, whereby it turns out that axial stress transfer is much more important. Hence, one may expect that decoupling of the fibre takes place at the fibre ends first.

The relation between the magnitude of shear stress transfer and the ratio of elastic moduli is approximately

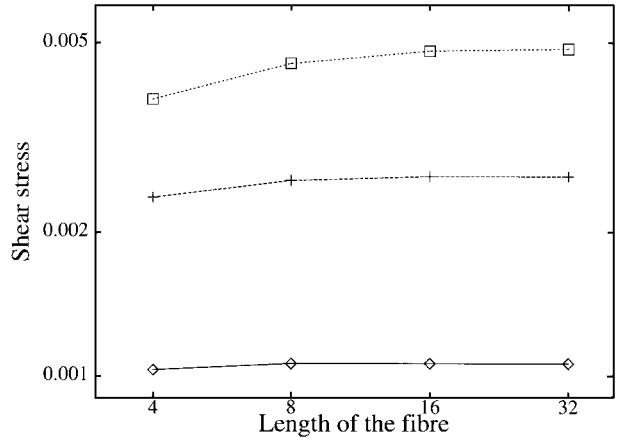

Figure 7 Interfacial shear stresses, σ_{xy}, between the fibre and the matrix. $w_f = a$; lines from top to bottom correspond to $\delta = 8$, 4 and 2.

linear, whereas in previous results [13] the interfacial shear stresses grow more slowly with δ. The discrepancy is probably due to the small system width used in the previous work.

3.1.4. Stresses in the fibre

As mentioned in the Section 1, the distribution of axial stresses, σ_f, in a fibre embedded in a matrix has been studied experimentally and found for low strains and perfect adhesion at the interphase boundary to conform well to the cosh-form given by the shear-lag theory [5]. Related numerical studies have been done with random fibre networks, the elastic properties of which have been modelled with shear-lag-type approaches [5], which, however, appear to overestimate the elastic modulus [8]. The cosh-form for $\sigma_f(x)$ was found to be obeyed for fibres oriented in the direction of external strain [8, 24, 25]. Moreover, in reinforced fibre networks, i.e. networks in which a low volume fraction of fibres with high elastic modulus are placed into a random fibre network, the maximum of $\sigma(x)$ is proportional to the ratio of elastic moduli of the fibre and the background [25].

In the following we study the maximum stress in the fibre as well as the shape of the axial stress distribution. Fig. 8 shows the shape of the axial stress along the fibre axis. The shortening of the flat stress maximum in the fibre with increasing δ for constant l_f is clearly visible. This, of course, corresponds to growth of l_c with δ. Most theoretical approaches yield the relation

$$l_c \propto (\delta)^{1/2} \tag{5}$$

(for a review, see [6]), but some numerical simulations suggest a linear dependence instead [11, 13]. We have not studied the dependence of l_c on δ systematically, but our data are consistent with Equation 5. In determining l_c, the criterion for σ_f to attain the maximum value was chosen to be 97% of $E_f\epsilon_x$.

Next, we embark on a study of the magnitude of the maximum of $\sigma(x)$. For a solitary fibre in a matrix, the maximum has the limiting value of $E_f\epsilon_x$, but falls below this "ideal limit" for short fibres. Fig. 9 shows that for $E_f \leq E_{bg}$, σ_f^{max} and δ are approximately linearly related. This is also a good approximation for stresses in fibres longer than l_c. When $l_f < l_c$ and the elastic modulus of the fibre is higher than that of the matrix, the relation

$$\sigma_f^{max} \propto \ln \frac{E_f}{E_{bg}} \tag{6}$$

applies approximately. Thus the logarithmic dependence of the pressure increase, α, on the ratio of the moduli can be related to the behaviour of the maximum axial stress of the fibre. Moreover, the same functional dependence was observed for the maximum stress in reinforcement fibres in fibrous networks [25], whereby it can be deduced that in that case the length of the fibre was below the critical one. Below we discuss the reasons for the observed $\sigma_f^{max}(\delta)$ dependence for fibres shorter than the critical length.

Let us have a look at the prediction of the shear-lag theory [5], which–apart from axial stress transfer at fibre ends–is a good model for the axial stress in the fibres at the dilute limit [23]. From Equations 1 and 2 one can obtain predictions for dependence of the magnitude of $\sigma_f^{max}(x)$ on δ as

$$\sigma_f^{max} \propto \delta\left[1 - \frac{c_1}{\cosh 1/(\delta)^{1/2}}\right] \tag{7}$$

where c_1 is a constant.

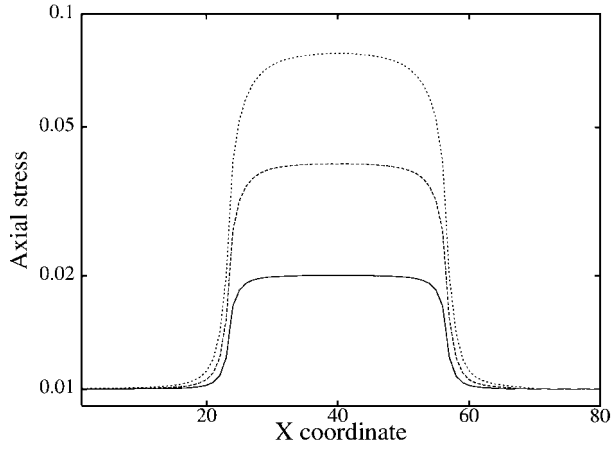

Figure 8 Axial stresses in the fibre for $w_f = 2a$ and $l_f = 32a$. The three lines are, from top to bottom, $E_f = 8$, 4 and $2E_{bg}$.

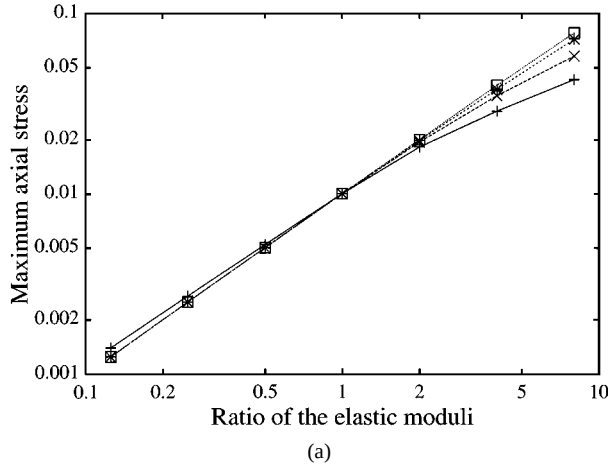

(a)

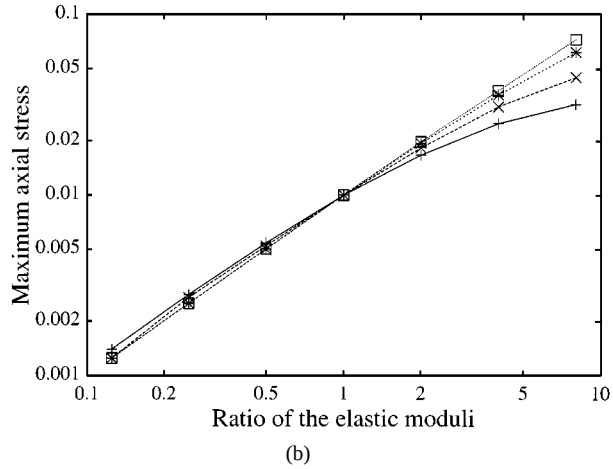

(b)

Figure 9 Maximum axial stress in the fibre as a function of the ratio of the elastic moduli of the fibre and the background. $w_f = a$ (a) and $2a$ (b). The four curves presented correspond to $l_f = 4a$ (+), $8a$ (×), $16a$ (∗) and $32a$ (□). Straight lines correspond to linear $\sigma_f^{max}(\delta)$-relation.

The above equation turns out to be inadequate for giving a full account of the type of relation given in Equation 6. The reason for this is, simply, axial stress transfer takes place at the ends of the fibre, giving rise to deviation of σ_f from the cosh-form and changing the value of σ_f^{max}. Because the axial stress transfer increases with both increasing δ and increasing l_f (the latter up to l_c, Fig. 4), the effect of axial stress transfer at fibre ends on axial fibre stress is non-trivial.

A simple argument will be presented, which is basically similar to the one used by Hsueh [9], to extend the shear-lag theory to include axial stress transfer. Our crucial ingredient is the knowledge of the dependence of pressure increase, α, on δ. Let us assume that $l_f < l_c$, whereby the theoretical maximum stress is not attained, i.e. the expression in parentheses in Equation 7 is smaller than unity. The axial stress transferred to the fibre from the matrix is approximately proportional to the logarithm of the ratio of the elastic moduli (Fig. 4), or $\sigma_{ax} \propto \ln \delta$. The axial stress in the fibre can be modelled as being of cosh-form-type added to σ_{ax}. Thus one may write

$$\sigma_f^{max} \propto \left\{ (E\epsilon_x - \phi \ln \delta)\left[1 - \frac{c_1}{\cosh 1/(\delta)^{1/2}}\right] + \phi \ln \delta \right\}$$
$$= E\epsilon_x \left[1 - \frac{c_1}{\cosh 1/(\delta)^{1/2}}\right] + \frac{\phi \ln \delta}{\cosh 1/(\delta)^{1/2}} \quad (8)$$

where ϕ is a constant determining the importance of axial stress transfer. Please observe that for $l_f < l_c$, σ_f^{max} can be larger when axial stress transfer takes place. The latter term in Equation 8 grows in importance with increasing ϕ, and provides an explanation for the dependence of σ_f^{max} of the type of Equation 6.

Summarizing the current section, the maximum axial stress in the fibre, σ_f^{max}, for fibre lengths shorter than the critical value is not given correctly by pure shear-lag theory. By using the knowledge presented in Section 3.1.3. that axial stress transfer has approximately a logarithmic dependence on the ratio, δ, of the elastic moduli of the fibre and the background, an axial stress transfer term can be incorporated in the shear-lag model in a simple way. With this addition, we obtain a qualitatively correct relation between σ_f^{max} and δ.

3.1.5. Grid size dependence of results

We tested the dependence of the results on the grid size by comparing $l_f = 16a/L = 80$ with $l_f = 8a/L = 40$ ($w_f = 2a$). In the tests, all the x-co-ordinate values from the former results were divided by two in order to obtain a comparison between a "basic" case and one in which the linear size of the mesh was two times that of the basic case. The largest difference was found in the maximum axial stress, which was 9% lower for the coarser grid. (For other parameter values the difference was within 2%.) Matrix stresses next to the fibre, on the other hand, were the same in both cases, within 2%.

3.2. Tilted fibres

In this section we study fibres that are not oriented in the direction of external strain. Due to limitations imposed by discrete cubic lattice representation of fibres, we limit ourselves to studying fibres at an angle of $\pi/4$ with respect to the external strain. For the same reasons we only study fibres with $w_f > 3a$. A dramatic example of pressure field changes is shown in Fig. 10; please note especially the asymmetry of changes with respect to the fibre axis in the vicinity of the fibre. The quantity l_f^x is the projection of the fibre length in the direction of external strain, i.e. $l_f^x = l_f/(2)^{1/2}$. A corresponding definition applies to w_f^x.

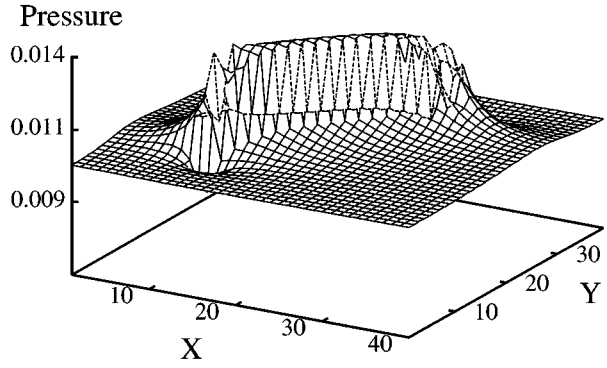

Figure 10 Pressure in the matrix and in the fibre tilted at an angle of $\pi/4$ with respect to the external strain. $L = 40$, $l_f^x = 16 \times a$, $w_f^x = 4 \times a$ and $\delta = 2$.

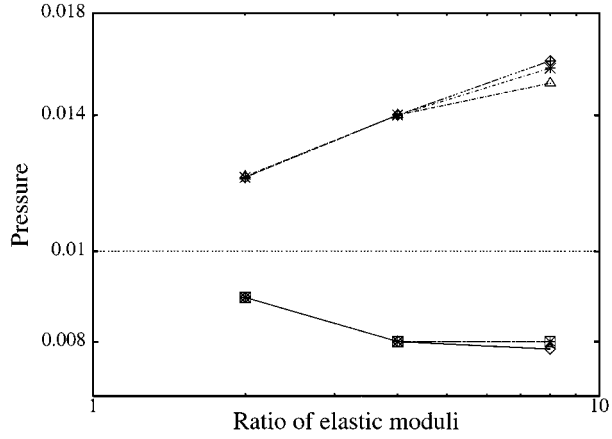

Figure 11 Change in matrix pressure in the vicinity of the fibre as function of δ. Shown are data for $l_f^x = 4a$, $8a$, $16a$ and $l_f = 32a$. $w_f^x = 4a$ in all cases. Both pressure increase (△) and pressure decrease (□) (those displaying a deviation from the general tendency of data) correspond to $l_f^x = 4a$. (∗) $l_f^x = 8a$.

Fig. 11 shows the magnitude of the pressure changes next to fibre ends as a function of the ratio of the elastic moduli, δ. The first observation is that for long enough fibres the magnitude of pressure changes does not depend on fibre length. Second, the increase of pressure next to the fibre end, $\alpha_1 p$, and corresponding reduction, $\alpha_2 p$, are roughly speaking "logarithmically symmetric" especially for small values of δ, i.e. $\alpha_1\alpha_2 = c(\delta) \approx 1$. The values for c are 1.07, 1.16 and 1.28 for $\delta = 2$, 4 and 8, respectively. The values do not depend on l_f, with the exception of the last value being 1.2 for $l_f = 4a$.

To complete the current account of the oblique fibre case, Fig. 12 shows the dependence of pressure decrease next to fibre ends as a function of fibre width. We show only the case of $l_f^x = 32a$, but the fibre length turns out not to affect the results. In the curves, after $w_f^x = 2a$

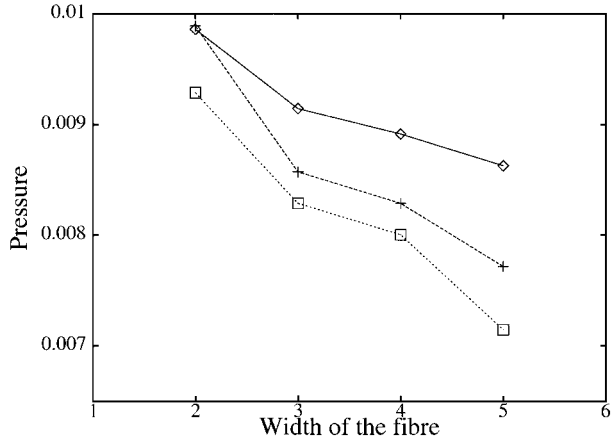

Figure 12 Decrease in matrix pressure next to the fibre ends as a function of w_f^x. $L = 80$, $l_f^x = 32a$. The three curves are, top to bottom, $\delta = 2$, 4 and 8.

a sudden drop is seen, but after that the behaviour is approximately linear. The change may be related to discretation of the fibre in the oblique case: for a fibre with $w_f^x = 2a$ the local bending stiffness varies more than for e.g. $w_f^x = 3a$. This can be seen clearly from the fact that the pressure changes are identical for $\delta = 2$ and $\delta = 4$ for the narrowest width tested.

3.3. Effect of fibre breaking

Next we study the effect of breaking of the fibre. This is a subject that clearly has interest from the experimental point of view: how are large stress enhancements created next to the breaking points?

The systems studied are exactly as before, except that we set the elastic moduli of the bonds at the middle of the fibre equal to zero. This gives rise to pressure increases in the matrix next to the weak point. In the following, we estimate these effects both for longitudinal and oblique orientations of the fibre with respect to external strain.

3.3.1. Longitudinal fibres

According to the numerical data, the length of the fibre has only a relatively weak effect on pressure increase next to the breaking point (Fig. 13). When the ratio of the elastic moduli is larger, however, increasing fibre length produces clearly larger stress enhancements next to the damaged point. In addition, for short fibres δ has little effect on the magnitude of the pressure increases. With "large" values of l_f, the difference becomes obvious. The conclusion to be drawn from these facts is quite simply that for fibres shorter than $2 \times l_c$, breaking of the fibres does not have as drastic an effect on

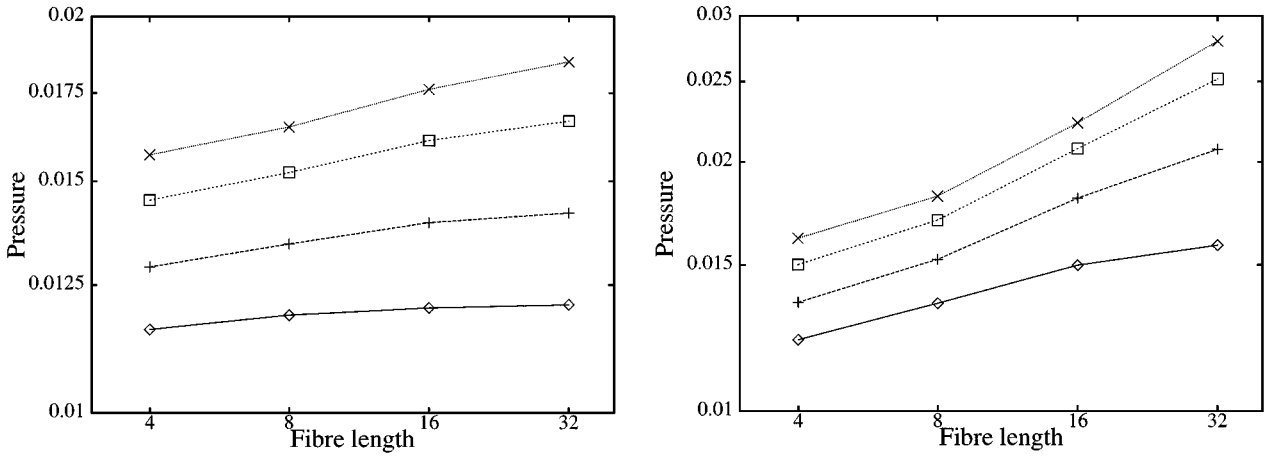

Figure 13 Height of the pressure increases next to the break in the fibre: (a) $\delta = 2$, and (b) $\delta = 8$. The different curves correspond to $w_f = 1$, 2, 3 and $4 \times a$ in the order of increasing pressure. Please note the difference in the vertical scales of the two plots.

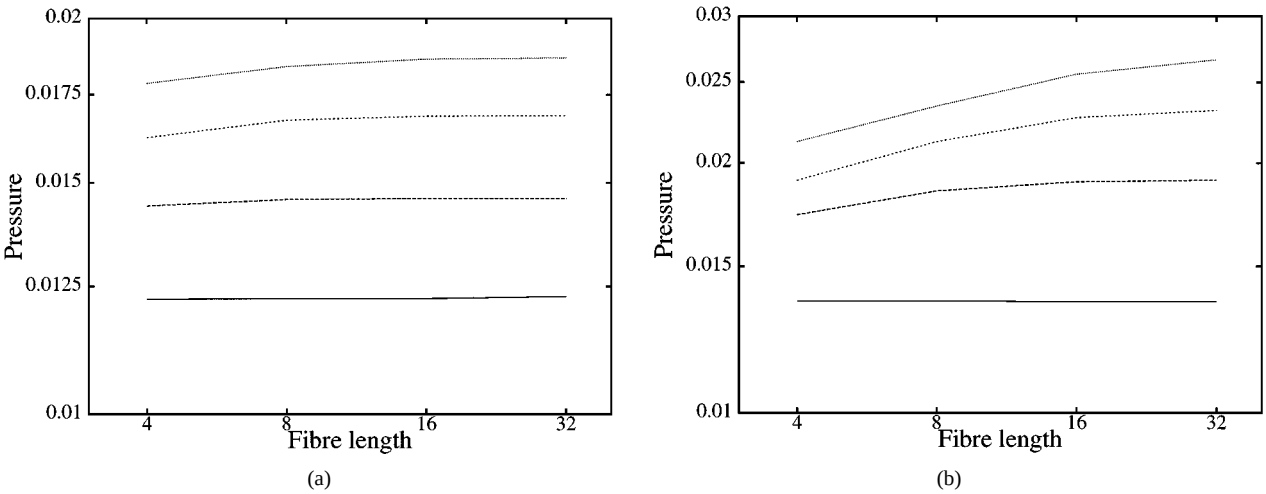

Figure 14 As Fig. 13, but for an oblique fibre. The fibre width and length are projected values.

the matrix pressure state as for longer fibres. On a more non-trivial note, it is seen that the pressure increase does *not* saturate, although the lengths of the fibre halves exceed the critical value. Furthermore, comparison of the data with Fig. 4 reveals that the magnitude of pressure increases next to the breaking point is larger than that next to the fibre ends for small δ, i.e. for $l_f \gg l_c$. If the fibre is shorter than the critical length, however, the largest stresses take place at the ends of the fibre even in the case of fibre breaking.

3.3.2. Oblique fibres

The fracture in an oblique fibre was realized by effectively removing bonds belonging to the fibre at $x = L/2$ in a plane perpendicular to the external strain. The results for pressure increases next to the fracturing point are similar to those presented above for a fibre oriented parallel to the external strain (Fig. 14). Notably, however, the magnitude of the increases in the pressure are smaller, especially for narrower fibres. This can be attributed to shear stresses, which tend to straighten the two halves of the fibre being distributed on an area, which is large in comparison with the almost point-like pressure "hot spot" seen in the breaking of a longitudinal fibre. Moreover, for a short fibre, the pressure increases next to the breaking point are smaller for an oblique fibre than for one oriented in the direction of the external strain. For longer fibres, on the other hand, tilting of the fibre does not have much effect.

4. Conclusions

The stress transfer between a solitary fibre and an elastic matrix was studied numerically. We parameterize the stress transfer using the length and the width of the fibre, as well as δ, the ratio of the elastic moduli of the fibre and the background. For fibre lengths, l_f, shorter than the critical one, l_c, it is observed that axial stress transfer at fibre ends shows a behaviour that is consistent with a logarithmic dependence on δ.

For fibres shorter than the critical length, the dependence of maximum axial stress of a fibre on the ratio of the elastic moduli is not linear. A purely shear-lag-type model can not account for this relation due to axial stress transfer at fibre ends. The addition of an axial stress transfer term proportional to $\ln \delta$ yields qualitatively correct behaviour. The far field of the fibre can be well modelled with dipole form, also for fibres with non-vanishing width.

The results are based on a model in which adhesion both along the fibre and at fibre ends is perfect and no debonding takes place during loading. If there is debonding at the ends of the fibre, the critical length increases [26] and obviously also axial stress concentrations next to the fibre ends decrease. Interfacial debonding along the length axis of the fibre diminishes stress transfer between the fibre and the matrix, thereby causing the fibre to have less effect on the stress state of the matrix.

Study of the breaking of a fibre into two parts of equal length shows that the pressure increase in the matrix next to the damaged point in the fibre is larger than pressure change at the ends of the unbroken fibre when the ratio of the elastic moduli, δ, is small. Tilting of the fibre plays down pressure increases for short fibres, but not for long ones.

The results for the shape of the stress fields of fibres will be applied to the study of the effect of texture on the mechanical properties of short-fibre reinforced composites in a forthcoming publication. Possible interesting future directions also include study of interface delamination for a fibre at an angle with respect to the external strain.

Acknowledgements

VIR thanks the Finnish Cultural Foundation and the Academy of Finland for financial support. The authors wish to express their gratitude to the participants of the SFB 381 programme for interesting discussions and comments.

References

1. Z. HASHIN, *J. Appl. Mech.* **50** (1983) 481.
2. W. A. CURTIN, *Phys. Rev. Lett.* **80** (1998) 1445.
3. M. IBNABDELJALIL and W. A. CURTIN, *Int. J. Solids Struct.* **34** (1997) 2649.
4. S. J. ZHOU and W. A. CURTIN, *Acta Metall. Mater.* **43** (1995) 3093.
5. H. L. COX, *Brit. J. Appl. Phys.* **3** (1952) 72.
6. I. M. ROBINSON and J. M. ROBINSON, *J. Mater. Sci.* **29** (1994) 4663.
7. L. MONETTE, M. P. ANDERSON and G. S. GREST, *J. Appl. Phys.* **75** (1994) 1155.
8. V. I. RÄISÄNEN, M. J. ALAVA, K. J. NISKANEN and R. M. NIEMINEN, *J. Mater. Res.* **12** (1997) 2725.
9. C. H. HSUEH, *J. Mater. Sci.* **24** (1989) 4475.
10. *idem, ibid.* **30** (1995) 219.
11. M. MURAT, M. ANHOLT and D. H. WAGNER, *J. Mater. Res.* **7** (1992) 3120.
12. Y. TERMONIA, *J. Mater. Sci.* **22** (1987) 1733.
13. *idem, ibid.* **22** (1987) 504.
14. L. MONETTE, M. P. ANDERSON, S. LING and G. S. GREST, *ibid.* **27** (1992) 4393.
15. Y. TERMONIA, *ibid.* **25** (1990) 4644.
16. L. MONETTE, M. P. ANDERSON and G. S. GREST, *ibid.* **28** (1993) 79.
17. F.-G. BUCHHOLZ and O. KOCA, *Comp. Mater. Sci.* **9** (1997) 18.
18. O. KOCA and F.-G. BUCHHOLZ, *ibid.* **3** (1994) 135.
19. A. HANSEN, in "*Statistical Models for Fracture of Disordered Media*," edited by H. J. Herrmann and S. Roux (North-Holland, Amsterdam, 1990).
20. G. N. HASSOLD and D. J. SROLOVITZ, *Phys. Rev.* **B39** (1989) 9273.
21. S. ROUX, *J. Physique Lett.* **46** (1985) L999.
22. H. J. HERRMANN, A. HANSEN and S. ROUX, *Phys. Rev.* **B39** (1989) 637.
23. M. C. ANDREWS, R. J. DAY, X. HU and R. J. YOUNG, *Mater. Sci. Lett.* **11** (1992) 124.
24. J. ÅSTRÖM, S. SAARINEN, K. NISKANEN and J. KURKIJÄRVI, *J. Appl. Phys.* **75** (1994) 2383.
25. V. I. RÄISÄNEN, S. HEYDEN, P.-J. GUSTAFSSON, M. J. ALAVA and K. J. NISKANEN, *Nordic Pulp Paper Res. J.* **12** (1997) 162.
26. C. H. HSUEH, R. J. YOUNG, X. YANG and P. F. BECHER, *Acta Mater.* **45** (1997) 1469.

Received 1 June
and accepted 21 July 1998